NEW ZEALAND SOCIETY FOR EARTHQUAKE ENGINEERING
2019 Pacific Conference on Earthquake Engineering
TURNING HAZARD AWARENESS INTO RISK MITIGATION
4 – 6 April | SkyCity, Auckland | New Zealand

FEM prediction of failure mechanisms in RC structural walls: parametric investigation

F. Dashti & R.P. Dhakal
University of Canterbury, Christchurch, New Zealand.

S. Pampanin
Sapienza University of Rome, Italy.

ABSTRACT

This study investigates the ability of a microscopic (finite element) model based on curved shell element formulation in predicting nonlinear behavior of planar RC structural walls, identifying the strengths and limitations of this modeling approach. For this purpose, a parametric validation is conducted in addition to verification of the model simulation against experimental results of several wall specimens tested in literature. The effects of variations in total length, thickness, shear-span ratio, axial load ratio, confinement, as well as the horizontal and vertical reinforcement ratios are investigated at both global and local levels. The capabilities and deficiencies of the modelling approach are discussed in detail in light of the numerical vs experimental as well as parametric verifications. The model is found to be able to predict most of the experimentally observed failure mechanisms of rectangular walls including global out-of-plane instability under in-plane loading, concrete crushing at the base, diagonal tension and diagonal compression as well as sliding shear. The model is not able to represent bar buckling, bar fracture and the potential subsequent secondary failure modes such as instability of the compression boundary zone due to progressive asymmetric concrete crushing at the base. The parametric study indicated sensitivity of the model response to the variation of the parameters known to be influential on the in-plane and out-of-plane responses of RC walls.

1 INTRODUCTION

Despite significant advances in the numerical solution methods and the availability of high-speed computing machines, simulation of all the failure mechanisms observed in reinforced concrete structures is still a complex task. On the other hand, size restrictions of the laboratories as well as limitations of the loading facilities put limits on the dimensions of the test specimens. With the prototype models designed taking these restrictions into account, dimensions of the wall specimens (particularly wall length) are remarkably smaller than the ones designed and constructed in real practice. Therefore, the numerical prediction is still considered as an alternative for investigating the seismic response of structural walls.

Dashti et al. (2014a, 2014b) proposed a microscopic (FEM) modeling technique using curved shell elements available in DIANA commercial program for numerical modeling of structural walls. The model could reasonably simulate nonlinear response of structural walls and predict the out-of-plane deformation that was observed in several rectangular wall specimens under in-plane loading. Parra (2016) used this modeling approach to investigate the out-of-plane response of wall units and the corresponding boundary zones. Rosso et al. (2017) simulated the response of thin RC columns prone to out-of-plane instability using this method. Scolari (2017) compared the out-of-plane response captured by PARC_CL 2.0 crack model with the one predicted by this model. A validation of the model was conducted by Dashti (2017) and Dashti et al. (2017, 2018a, 2018b) which mainly focused on verification of the out-of-plane instability simulated by the model using results of several tested wall specimens as well as a blind prediction practice.

The response of several wall specimens that exhibited various failure mechanisms in the laboratory were simulated by several modeling approaches within the modeling group of the Virtual International Institute for Performance Assessment of Structural Wall (NSF SAVI Wall Institute). Different macroscopic and microscopic model formulations were validated against these specimens that reflected a broad range of wall configurations and response characteristics (Kolozvari et al. 2018a, 2019). One of the microscopic (FEM) modeling techniques involved using curved shell elements available in DIANA commercial program. However, not all the features of wall response used for the verification practice could be included in Kolozvari et al. (2018b) and further details on strengths and limitations of this modeling approach are presented in a more comprehensive study (Dashti et al. 2019). Dashti et al. 2019 extended the simulation practice conducted using this method to parametric investigations on the observed failure patterns. For this purpose, sensitivity of the wall models to a set of parameters known to be influential on evolution of different failure mechanisms in structural walls was investigated. The correlation of shear-span ratio, confinement length, longitudinal and horizontal reinforcement ratio, axial load ratio as well as wall dimensions with some of the response characteristics of structural walls was investigated. These response features included the contribution of shear and flexural displacement components to the total top displacement at different stages of loading, strain gradients along the length and height of the wall, principal stress and strain distributions, axial growth and out-of-plane response. In this paper, a summary of the extensive validation and parametric study conducted by Dashti et al. (2019) on the global and local response prediction of the curved shell finite element model is presented.

2 ANALYSIS MATRIX

The analysis matrix designed for parametric evaluation of the model generated for Specimens RW2, SP4, R2, WSH6 and S6 is summarized in Table 1. Specimen RW2 (Thomsen IV and Wallace 1995) was a relatively slender RC wall characterized with a shear-span ratio of 3.1, axial load of $0.09A_g f'_c$, and a low shear stress demand of $0.22\sqrt{f'_c}$ MPa ($2.7\sqrt{f'_c}$ psi) at flexural capacity, which experienced flexural failure due to crushing/buckling at the wall boundaries. The effects of shear-span ratio, axial load ratio, confinement length and total length of the wall are investigated using Models RW2-SS, RW2-A, RW2-CA and RWL, respectively. The height of RW2-SS and consequently its shear-span ratio are almost half of the ones of

RW2. RW2-A is subjected to an axial load that is two times greater than the one applied to RW2. Under this high axial load, the confinement length is reduced by 50% (denoted as RW2-CA) to highlight the importance of confinement along the neutral axis depth. RW2-L represents a wall that is longer compared to RW2 but has all the other features, such as shear-span ratio, confinement ratio, etc. identical to RW2. Therefore, the height and confinement length of the wall are increased in order to keep these ratios constant. These models are subjected to higher drift levels (up to 3.0%) as compared to the 2.5% drift applied to the test specimen to more effectively capture the trend by with the model response varies at higher drift levels.

RW-A15-P10-S78 (referred to as SP4 for brevity) (Tran and Wallace 2015) was a medium-rise RC wall with a shear-span ratio of 1.50, axial load of 0.10Agf'c, and high shear stress demand of 0.65√f'c MPa (7.8√f'c psi), which experienced significant shear-flexural interaction and diagonal compression failure. The shear-span ratio, axial load ratio and the horizontal reinforcement ratio are considered as the variables for parametric study of Specimen SP4. The shear-span ratio of the benchmark specimen (SP4) is 1.5, and its response is consequently affected by shear deformation. Therefore, the parameters are chosen such that they induce variation of shear demand and capacity on the model. SP4-SS1 and SP4-SS1 represent lower (0.75) and higher (3.0) shear-span ratios, respectively. SP4-A was subjected to an axial load ratio two times greater than the one applied to SP4. The ratio of the horizontal reinforcement in SP4-HRe was half of the one in SP4.

Table 1: Analysis matrix for parametric investigation of Specimens RW2, SP4, R2, WSH6, S6

		H_w	L_w	CL	CL/ L_w	t	f'_c (MPa)	f_{yBE} (MPa)	ρ_{vBE} (%)	$\rho_{h,web}$/ $\rho_{v,web}$ (%)	M/(VL_w)	P/($A_g f_c$)
Benchmark	RW2	3660	1219	191	0.16	102	34.0	434	2.93	0.33/0.33	3.13	0.09
1	RW2-SS	2000	1219	191	0.16	102	34.0	434	2.93	0.33/0.33	1.64	0.09
2	RW2-A	3660	1219	191	0.16	102	34.0	434	2.93	0.33/0.33	3.13	0.18
3	RW2-C-A	3660	1219	96	0.08	102	34.0	434	2.93	0.33/0.33	3.13	0.18
4	RW2-L	6125	2040	320	0.16	102	34.0	434	2.93	0.33/0.33	3.13	0.09
Benchmark	SP4	1829	1219	229	0.19	152.4	55.8	477	6.06	0.73/0.73	1.5	0.1
1	SP4-SS1	915	1219	229	0.19	152.4	55.8	477	6.06	0.73/0.73	0.75	0.1
2	SP4-SS2	3658	1219	229	0.19	152.4	55.8	477	6.06	0.73/0.73	3.0	0.1
3	SP4-A	1829	1219	229	0.19	152.4	55.8	477	6.06	0.73/0.73	1.5	0.2
4	SP4-HRe	1829	1219	229	0.19	152.4	55.8	477	6.06	0.37/0.73	1.5	0.1
Benchmark	R2	4572	1905	187.3	0.10	101.6	46.4	450	4.00	0.31/0.25	2.40	0.00
1	R2-T	4572	1905	187.3	0.10	11.6	46.4	450	4.00	0.31/0.25	2.40	0.00
Benchmark	WSH6	4520	2000	385	0.19	150	45.6	576	1.54	0.25/0.54	2.26	0.11
1	WSH6- Re	4520	2000	385	0.19	150	45.6	576	4.62	0.25/0.54	2.26	0.11
Benchmark	S6	2095	2412	279	0.12	114	27.8	482	5.6	0.55/0.55	1.6	0.05
1	S6-A	2095	2412	279	0.12	114	27.8	482	5.6	0.55/0.55	1.6	0.15

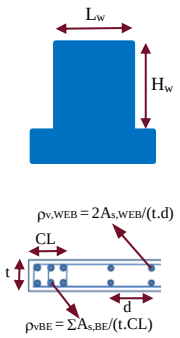

* Dimensions in mm

R2 (Oesterle et al. 1976), was a relatively slender RC wall, with an aspect ratio of 2.35, no axial load, and a low shear stress demand of 0.17√f'c MPa (2.1√f'c psi), which exhibited out-of-plane instability. WSH6 (Dazio et al. 2009) was a moderately slender RC wall specimen with an aspect ratio of 2.02, axial load of 0.11Agf'c, and low shear stress demand of 0.3√f'c MPa (3.6√f'c psi), which failed due to crushing of the compression zone caused by fracture of a number of confining hoops and buckling of the longitudinal boundary reinforcement. S6 (Vallenas et al. 1979) was a moderately slender RC wall with a shear span ratio of 1.60, axial load of 0.06Agf'c, and a relatively large shear stress demand of 0.53√f'c MPa (6.4√f'c, psi). Failure of this specimen was triggered by spalling of concrete cover on only one side of the boundary element, which resulted in out-of-plane buckling of the boundary element after spalling of the concrete cover at a story drift of 1.93%. The parametric verification of the models for Specimens R2, WSH6 and S6 is conducted using one parameter per specimen for the sake of brevity. As elaborated in Dashti et al. (2018a), the numerical model could simulate the out-of-plane instability failure of Specimen R2, and the unsupported

height to thickness ratio is known to be one of the major parameters controlling this mode of failure. Therefore, the thickness is slightly increased in the numerical model to evaluate sensitivity of the response to this parameter. WSH6 had a low reinforcement ratio in the boundary regions and was predicted to have a rather pinched response. The reinforcement content was therefore doubled in WSH6-Re, and the numerical model of Specimen S6 was subjected to an axial load three times as much as the one applied in the test (denoted as S6-A).

3 EXPERIMENTAL VERIFICATION AND RESPONSE OF THE PARAMETRIC MODELS

Load-displacement response of the numerical models generated for Specimen RW2 and Specimen SP4 are compared with the test results in Figure 1a and Figure 2a, respectively. The capability of the model in prediction of the contribution of shear and flexural displacement components to the total top displacement is evaluated in Figure 1b and Figure 2b. As can be seen in these figures, the displacement components of the numerical models are in reasonably good agreement with the test measurements and are, therefore, used for evaluation of the parametric models. Figure 1c and Figure 2c present the shear contribution plots of the parametric models generated for Specimens RW2 and SP4, respectively. The points corresponding to initiation of strength degradation in the load-displacement curves are indicated in these figures. It should be noted that the contribution plots correspond to the 1st cycle of each drift level and the cyclic degradation would obviously alter the values for the subsequent (2nd and 3rd) cycles at each drift level.

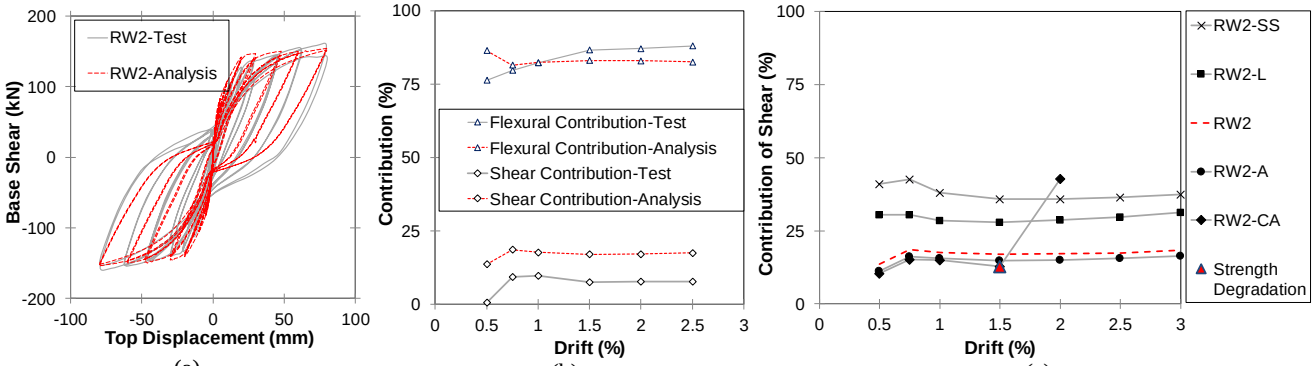

(a) (b) (c)

Figure 1: Experimental verification and response of the parametric models for Specimen RW2: (a) test vs analysis-load vs displacement; (b) test vs analysis- shear and flexural contribution; (c) contribution of shear displacements to the top displacement-parametric models

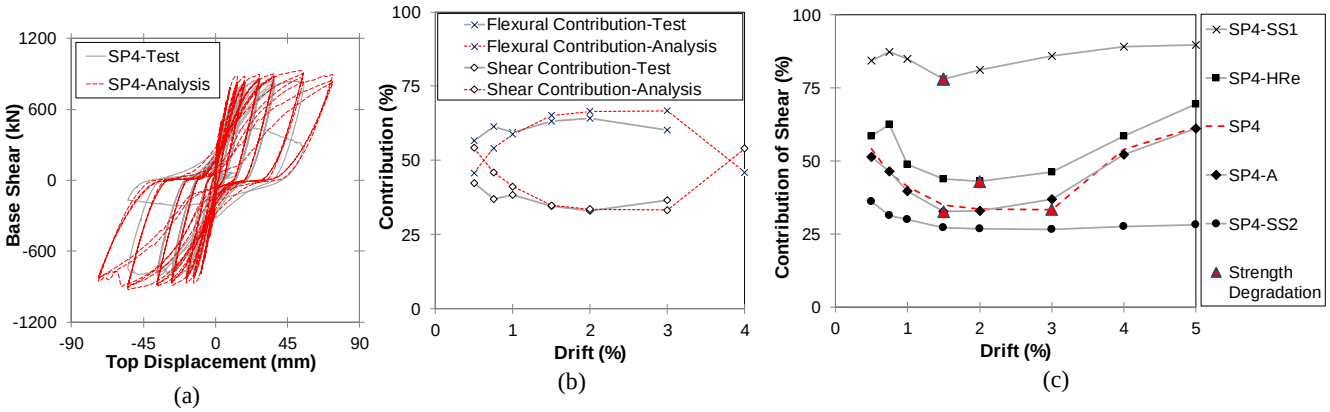

(a) (b) (c)

Figure 2: Experimental verification and response of the parametric models for Specimen SP4: (a) test vs analysis-load vs displacement; (b) test vs analysis- shear and flexural contribution; (c) contribution of shear displacements to the top displacement-parametric models

As can be seen in Figure 1c, contribution of shear displacement to the top displacement increased by 20% when the shear-span ratio of RW2 decreased by about 50%, RW2-SS, causing the same amount of decrease in the flexural displacement. Also, this contribution is not constant throughout the loading. The flexural contribution increased up to 1.5% drift and started to gradually decrease afterwards (i.e., the shear contribution started to increase after 1.5%). As for the increase in wall length for a constant shear-span ratio, RW2-L, the shear stress was increased leading to higher contribution of shear deformation to the total top displacement since the thickness was kept constant. The increase of axial load, RW2-A, did not have a big impact on the contribution of the shear and flexural displacements to the total top displacement, which led to minor increase of the flexural contribution and consequently slight decrease of the shear contribution. The decrease of confinement length under the increased axial load, RW2-CA, however, resulted in noticeably large increase of shear deformation and initiation of failure at 1.5% drift.

According to the contribution plots of SP4, shown in Figure 2c reduction of the shear-span ratio from 1.5 to 0.75, SP4-SS1, resulted in dramatic increase in contribution of shear compared to that of SP4, and the shear failure of the model at 1.5% drift led to a rapid increase of the shear contribution. The decrease of the horizontal reinforcement ratio, SP4-HRe, did expectedly result in higher contribution of shear displacement. The shear contribution plot indicates steady increase of shear contribution starting at 2.0% drift as compared to the one in SP4 which initiated at 3.0% drift. The increase of axial load, SP4-A, apparently did not have a big impact on the contribution percentage of shear and flexural displacements. The increase of shear contribution, however, started at a lower drift (1.5%), when the strength degradation started to develop. Although the variation of shear contribution due to the increase of shear-span ratio from 1.5 to 3.0, SP4-SS2, was not as noticeable as the one corresponding to SP4-SS1, no abrupt increase of shear contribution was noticed in this case and the response was expectedly flexure-dominated.

The load vs in-plane displacement prediction of the model for Specimen R2 is compared with the test measurements in Figure 3a along with the maximum out-of-plane displacement history of the model. This specimen had exhibited out-of-plane instability under in-plane loading. The progression of this mode of failure in rectangular walls is described in full detail by Dashti et al. (2018c). Figure 3b-d compare the response of the model with increased thickness (R2-T) with the benchmark model (R2). Unlike R2, the analysis of R2-T was not terminated due to instability during the 2.2% drift cycles and was continued up to the final loading stage. Figure 3c indicates that the slight increase of the wall thickness resulted in lower values of the out-of-plane displacement during all the applied drift levels. The axial growth plot, shown in Figure 3d, also shows the effect of large out-of-plane displacement on the drop of elongation in both models.

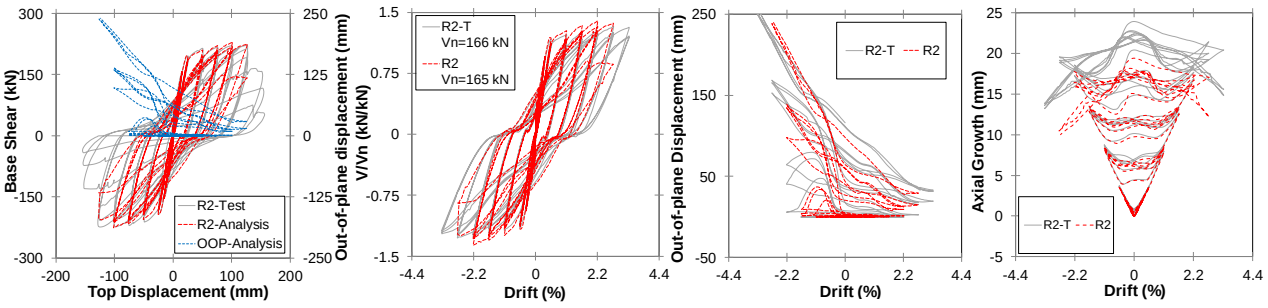

(a) (b) (c) (d)

Figure 3. Experimental verification and response of the parametric model for Specimen R2: (a) test vs analysis-load vs displacement (b) parametric model-load vs displacement; (c) parametric model-maximum out-of-plane displacement; (d) parametric model-axial growth

The load vs in-plane displacement prediction of the model for Specimen WSH6 is compared with the test measurements in Figure 4. The reinforcement content was doubled in WSH6-Re which understandably resulted in higher flexural capacity and yield drift (Figure 4b). The shear demand was therefore increased significantly leading to noticeable increase in the shear contribution plot as compared to that of the

benchmark model (Figure 4c). The tensile strain gradient along the boundary region height (Figure 4d) was also affected and lower vertical strains were developed in the extreme end boundary region longitudinal reinforcement.

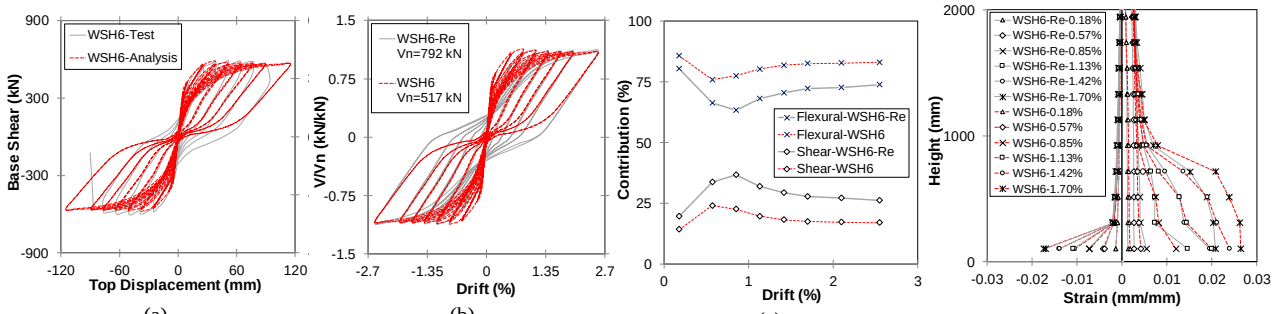

(a) (b) (c) (d)

Figure 4. Experimental verification and response of the parametric model for Specimen WSH6: (a) test vs analysis-load vs displacement (b) parametric model-load vs displacement; (c) parametric model- shear and flexural contribution; (d) parametric model- strain gradients along the height

The load vs in-plane displacement prediction of the model for Specimen S6 is compared with the test measurements in Figure 5. The model with three times higher axial load (S6-A) failed due to diagonal compression during the first 1.3% drift cycle (Figure 5b), followed by shear sliding in the subsequent cycles. The contribution plot, shown in Figure 5c, displays a rapid increase of shear deformation caused by this failure pattern. The minimum principal stress distribution of S6-A is compared with the one of S6 at the 1.3% drift along with the corresponding illustrations of the total principal strain (Figure 5d). The large compressive stresses developed in the panel under higher axial load (S6-A) resulted in evolution of concrete crushing in the panel region next to the compression boundary (the bright area that carries a negligible load). This web crushing followed by concrete crushing in the boundary region resulted in progression of shear sliding in the model. Comparison of the total principal strain contour for S6-A with the one of S6 shows initiation of this failure at 1.3% drift.

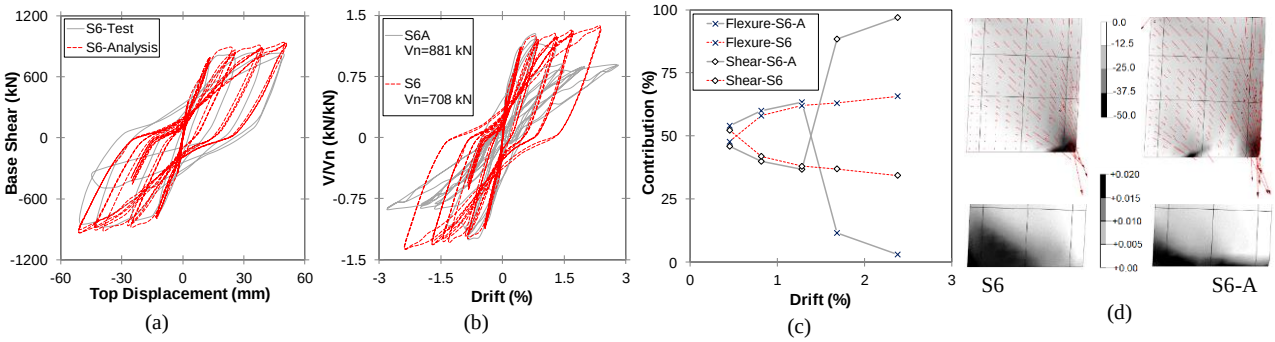

(a) (b) (c) (d)

Figure 5. Experimental verification and response of the parametric model for Specimen S6: (a) test vs analysis-load vs displacement; (b) parametric model-load vs displacement; (c) parametric model- shear and flexural contribution; (d) parametric model- distribution of minimum principal stress (S3, in MPa) and total principal strain E1 at 1.3% drift

4 SUMMARY AND CONCLUSIONS

A microscopic model based on curved shell element was validated in this study using parametric analysis approach. The sensitivity of the model response to variation of different parameters known to be influential on nonlinear response of structural walls was evaluated using test results of wall specimens that had exhibited a variety of failure modes. The parameters included shear-span ratio, axial load ratio, confinement length, horizontal and vertical reinforcement ratios, thickness and length. As this study focused only on evaluating capabilities of the model and not on parametric investigation of the nonlinear response in

structural walls, the parameters noted above were changed within a limited range and using few parametric models. The strengths and limitations of the model identified using the experimental and parametric verification described above are listed below:

- The lateral load versus top total displacement response can be predicted reasonably well in terms of the shape of the hysteretic curve and cyclic degradation. The initial stiffness is generally overestimated. This is particularly noticeable for the post-cracking stiffness although the cracking strength is not far-off in most cases. The peak strength in each cycle is generally overestimated. The maximum discrepancy was around 12% among the specimens used in this study. The pinching is overestimated in most cases. This could be attributed to overpredition of pinching in the shear displacement component.
- The numerical model is able to capture the contribution of shear and flexural displacement components to the total displacement reasonably well. Therefore, the effects of different parameters on the performance of two of the specimens (which had the largest and smallest shear-span ratios) were evaluated using the percentage of shear contribution at different drift levels.
- The model is able to represent the effects of shear-span ratio, axial load ratio, confinement length, horizontal and vertical reinforcement ratios, thickness and length on the variation of shear contribution to the total top displacement at different stages of nonlinear response of the wall. The effects of these parameters on the drift level corresponding to initiation of strength degradation and failure of the walls can also be predicted by the numerical model. The initiation of strength degradation is understandably in line with dramatic increase of the shear contribution to the total displacement. The influence of wall geometry on evolution of out-of-plane deformation under in-plane loading can also be reasonably predicted
- The failure patterns successfully predicted by the model include: i) concrete crushing in slender walls under high axial load and with low confinement; ii) global out-of-plane instability of slender walls under in-plane cyclic loading; iii) diagonal tension in shear-dominant walls (squat walls) with light horizontal reinforcement; iv) diagonal compression in shear-dominant walls (squat walls) with high shear stress; v) sliding shear preceded by development of concrete crushing along the web and boundary regions.
- The failure patterns not represented in the model include: i) bar buckling and the subsequent progressive concrete crushing; ii) bar fracture and the subsequent stress redistribution; iii) out-of-plane instability as the secondary failure mode triggered by bar buckling, asymmetric cover spalling, concrete crushing, etc.

5 REFERENCES

Dashti, F., Dhakal, R.P. & Pampanin, S. 2014a. Numerical simulation of shear wall failure mechanisms, *New Zealand Society for Earthquake Engineering (NZSEE) Annual Technical Conference, 21-23 March 2014*. Auckland, New Zealand.

Dashti, F., Dhakal, R.P. & Pampanin, S. 2014b. Simulation of out-of-plane instability in rectangular RC structural walls, *the Second European Conference on Earthquake Engineering and Seismology, 25-29 August 2014*. Istanbul, Turkey.

Dashti, F. 2017. *Out-of-plane Instability of Rectangular Reinforced Concrete Walls Under In-plane Loading*. PhD Thesis, Department of Civil and Natural Resources Engineering, University of Canterbury

Dashti, F., Dhakal, R.P. & Pampanin, S. 2017. Numerical Modeling of Rectangular Reinforced Concrete Structural Walls, *Journal of Structural Engineering*, Vol 143. doi:10.1061/(ASCE)ST.1943-541X.0001729

Dashti, F., Dhakal, R.P. & Pampanin, S. 2018a. Validation of a Numerical Model for Prediction of Out-of-plane Instability in Ductile Structural Walls under Concentric In-plane Cyclic Loading, *Journal of Structural Engineering*. doi:10.1061/(ASCE)ST.1943-541X.0002013

Dashti, F., Dhakal, R.P. & Pampanin, S. 2018b. Blind prediction of in-plane and out-of-plane responses for a thin singly reinforced concrete flanged wall specimen, *Bulletin of Earthquake Engineering*, Vol 16 427–458. doi:10.1007/s10518-017-0211-x

Dashti, F., Dhakal, R.P. & Pampanin, S. 2019. A parametric investigation on applicability of the curved shell finite element model to nonlinear response prediction of planar RC walls, *Bulletin of Earthquake Engineering (under review)*

Dashti, F., Dhakal, R. & Pampanin, S. 2018c. Evolution of out-of-plane deformation and subsequent instability in

rectangular RC walls under in-plane cyclic loading: Experimental observation, *Earthquake Engineering and Structural Dynamics*. doi:10.1002/eqe.3115

Dazio, A., Beyer, K. & Bachmann, H. 2009. Quasi-static cyclic tests and plastic hinge analysis of RC structural walls, *Engineering Structures*, Vol 31 1556-1571

DIANA. 2011. *Finite Element Analysis User's Manual - Release 9.4.4*, 9.4.4 edn. TNO DIANA,

Kolozvari, K. et al. 2018. Comparative Study of State-of-the-Art Macroscopic Models for Planar Reinforced Concrete Walls, *ACI Structural Journal*. doi:10.14359/51710835

Kolozvari, K. et al. 2019. State-of-the-art in Nonlinear Finite Element Modeling of Reinforced Concrete Walls, *Engineering Structures*, Under Review

Oesterle, R., Fiorato, A., Johal, L., Carpenter, J., Russell, H. & Corley, W. 1976. Earthquake Resistant Structural Walls: Tests of Isolated Walls, *Research and Development Construction Technology Laboratories*, Portland Cement Association.

Parra, P.F. 2016. *Stability of Reinforced Concrete Wall Boundaries*. University of California, Berkeley

Rosso, A., Jime´nez, L., Almeida, J. & Beyer, K. 2017. Experimental campaign on thin RC columns prone to out-of-plane instability: numerical simulation using shell element models, *VIII Congreso Nacional de Ingenieri´a Si´smica*, Barranquilla, Colombia

Scolari, M. 2017. *Implementation of PARC_CL 2.0 crack model for reinforced concrete members subjected to cyclic and dynamic loading*. University of Parma

Thomsen IV, J.H. & Wallace, J.W. 1995. *Displacement-based design of reinforced concrete structural walls: An experimental investigation of walls with rectangular and T-shaped cross-sections*. Department of Civil and Environmental Engineering, Clarkson University, Potsdam, N.Y.,

Tran, T.A. & Wallace, J.W. 2015. Cyclic testing of moderate-aspect-ratio reinforced concrete structural walls, *ACI Structural Journal*, Vol 112 653

Vallenas, J.M., Bertero, V.V. & Popov, E.P. 1979. *Hysteretic behaviour of reinforced concrete structural walls*. Earthquake Engineering Research Center, University of California, Berkeley.